Development and Launch of the Purdue Hybrid Rocket Technology Demonstrator

John Tsohas[1] , Brad Appel[2], Andrew Rettenmaier[3], Mike Walker[4], and Stephen D. Heister[5]

Purdue University, West Lafayette, IN, 47906

The Purdue University School of Aeronautics and Astronautics is developing a hybrid rocket technology demonstrator to serve as a test bed for technologies critical to the development of vehicles capable of delivering microgravity experiments to altitudes exceeding 100 km. These critical technologies include propulsion, structures, separation, recovery, ground support, avionics and guidance, navigation and control sub-systems. These technologies will be demonstrated sequentially over a series of test flights which will allow the designers to validate each of these sub-systems before adding more complexity, risk and features to the technology demonstrator. To date, three different hybrid rocket motors have been designed, manufactured and tested. In addition the Ground Support Equipment required for transferring the oxidizer to and from the flight-vehicle has been constructed and tested extensively during cold flow and hot-fire test operations. A Mobile Launch Platform was also developed for transporting the ground support equipment and for performing launch operations in designated areas. This paper details the design and development of a flight-weight, 900 lbf thrust, 90% hydrogen peroxide/LDPE hybrid rocket motor which was successfully hot-fire tested in vertical configuration a total of five times at the Purdue Vertical Rocket Test Facility. In addition the paper describes the successful launch of the 1st generation hybrid flight-vehicle which reached an altitude of 6,100 ft (Mach 0.6) in June 2009, making a first important step towards flight operations for this series of hybrid rocket technology demonstrators.

---

[1] Graduate PhD Student, School of Aeronautics & Astronautics, 701 W. Stadium Ave., Student Member
[2] Graduate Masters Student, School of Aeronautics & Astronautics, 701 W. Stadium Ave., Student Member
[3] Undergraduate Student, School of Aeronautics & Astronautics, 701 W. Stadium Ave., Student Member
[4] Graduate Masters Student, School of Aeronautics & Astronautics, 701 W. Stadium Ave., Student Member
[5] Professor, School of Aeronautics & Astronautics, 701 W. Stadium Ave., Associate Fellow

I. Introduction

The Purdue University School of Aeronautics and Astronautics is developing a hybrid rocket technology demonstrator to serve as a test bed for technologies critical to the development of vehicles capable of delivering microgravity experiments to altitudes exceeding 100 km. These critical technologies include propulsion, structures, separation, recovery, ground support, avionics, and guidance, navigation and control sub-systems. These technologies will be demonstrated sequentially over a series of test flights which allow the designers to validate the sub-systems before adding more complexity and risk to the technology demonstrators.

Since its initiation in 2004, the Purdue Hybrid Rocket Project has designed, manufactured and hot-fire tested hybrid rocket motors of 25 lbf, 250 lbf, and 900 lbf thrust levels, and has successfully conducted more than 40 hot-fire tests during the various phases of development. In addition the Hybrid Rocket Project has constructed and extensively tested the Ground Support Equipment (GSE) required for transferring the oxidizer to and from the flight vehicle during hot-fire and launch operations. A Mobile Launch Platform (MLP) was also developed for transporting the GSE and for launching the flight-vehicle in designated remote areas. Finally, the 1st generation hybrid flight-vehicle was successfully launched to an altitude of 6,100 ft (Mach 0.6) in June 2009, making a first important step towards flight operations for this series of hybrid rocket technology demonstrators.

Hybrid propulsion was chosen over liquid and solid propulsion due to cost, complexity and reliability constraints placed early in the design process. Hybrid propulsion offers simplicity, reliability, and overall lower development and operations costs in comparison to liquid propulsion systems. In comparison to solid propulsion, hybrids offer higher specific impulse and improved safety as well as shut-down and throttling capability. Hydrogen peroxide was chosen as the oxidizer due to its high density Isp and its non-toxic, and non-cryogenic properties. This leads to safer propellant handling procedures which helps reduce operation costs in comparison to other candidate oxidizers. In addition, Purdue University has the facilities as well as extensive experience with the use of hydrogen peroxide as a rocket oxidizer. Low density polyethylene (LDPE) and HTPB are the fuels of choice due to their relative high performance, material properties, and manufacturing attributes in comparison to other candidate hybrid fuels.

The hybrid flight-vehicle is powered by a 900 lbf thrust motor and is designed to attain altitudes in excess of 25,000 ft. For initial flight testing, the propellant feed system will operate in blow-down mode, followed by higher altitude flights using a pressure regulated system. The flight-vehicle is designed to interface with the Mobile Launch Platform (MLP) and to operate in conjunction with the Ground Support Equipment (GSE). Oxidizer transfer operations, as well as control and data acquisition is routed via the onboard avionics through umbilical cords directly to the GSE. Valve control and data acquisition is controlled via a laptop computer located at a distance of more than 1,500 ft away. The hybrid rocket technology demonstrator consists of four main systems:

1) Mobile Launch Platform – launch tower, launch rail, trailer, ground support equipment (GSE), control and data acquisition system.
2) Aero-structures – fins, fuselage, nosecone, oxidizer tank, structural support mounts, etc
3) Propulsion – motor assembly, nozzle, chamber, injector, manifold, feed plumbing, valves.
4) Avionics/Recovery – on-board flight computers, altimeters, relays, batteries, routers, etc. Ejection charges, main and drogue parachutes, recovery harnesses, pistons and anti-zipper devices.

As shown in Fig. 1, the vehicle consists of a 6" diameter by 15.9 ft length carbon-fiber aero-structure with carbon-fiber fins directly mounted to the outside of the airframe. The hybrid rocket motor is mounted inside the minimum diameter carbon-fiber aero-structure via a series of support rings. Located directly above the hybrid rocket motor is the main fire valve and the quick-disconnect (QD) assembly used for loading the hydrogen peroxide into the flight vehicle and for separating prior to launch. The oxidizer tank is connected directly above the QD, with a pressure transducer, pressure relief valve, and a remotely controlled vent valve on its forward bulkhead. The drogue parachute compartment is located above the booster section, followed by the avionics and main parachute sections. Finally, the nose cone which contains the on-board camera is located forward of the main parachute compartment. This paper details the design and test work performed on the propulsion, structures, trajectory, avionics and the launch support systems, followed by results from the launch to 6,100 ft.
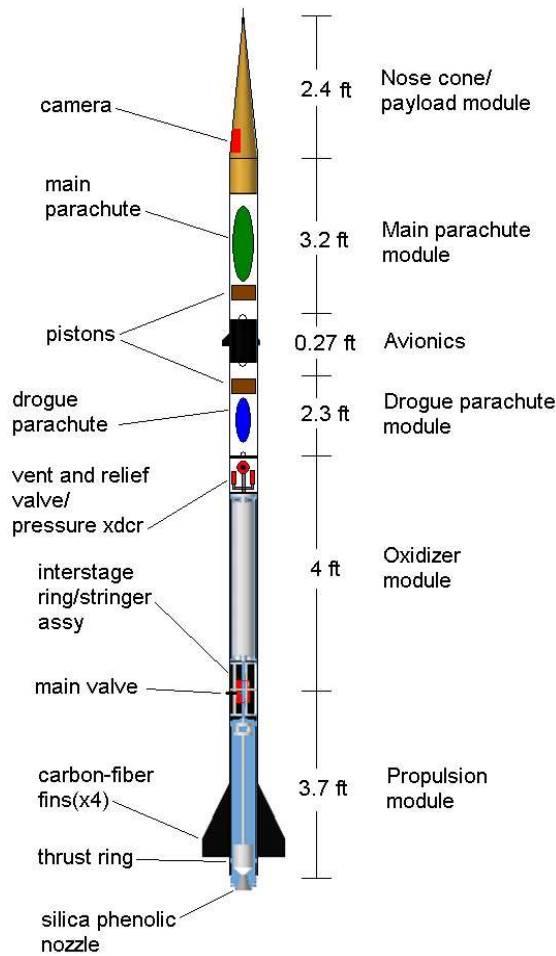
Figure 1. Schematic of hybrid propulsion flight-vehicle

II. Development and Testing of the 900 lbf thrust Flight-Weight Hybrid Rocket Motor

A. Design of the Flight-weight 900 lbf thrust Hybrid Rocket Motor

Prior to construction of the flight-weight 900 lbf thrust hybrid rocket motor, a series of hybrid rocket motors were designed, built and hot-fire tested at the Zucrow rocket test facilities. Initially, a 25 lbf thrust, subscale hybrid rocket motor was developed to acquire test data for characterization of 90% H_2O_2/HTPB performance and regression rate under hot-fire test conditions, and to validate the internal ballistics motor design code before attempting to scale up in thrust. A total of 10 hot-fire tests were conducted with the 25 lbf thrust motor.

The results from the 25 lbf thrust subscale motor tests were used to design and build a flight-weight 250 lbf thrust hybrid rocket motor which was hot-fire tested over 10 times to obtain important motor performance data. Following the 250 lbf thrust motor, a more powerful 900 lbf thrust, 4-port, hybrid rocket motor was designed for use on the Hybrid Rocket Technology Demonstrator. The motor uses 90% hydrogen peroxide oxidizer, low density polyethylene (LDPE) fuel, and is a 4-port derivative of the earlier 250 lbf H_2O_2/HTPB single-port motor. This 'battleship' motor featured thick steel walls and large welded flanges for its assembly, and was used as a workhorse for conducting over 15 successful hot-fire tests to build confidence in the four-port design before the flight-weight motor was designed. The aforementioned series of hybrid rocket motors are shown in Fig. 2.

American Institute of Aeronautics and Astronautics

Figure 2. Heritage motors for the flight-weight design. Hot-fire tests from the 25 lbf-thrust, 250 lbf-thrust, and 900 lbf-thrust hybrid rocket motors are shown from left to right.

The flight-weight 900 lbf-thrust motor is a virtual copy of the battleship 900 lbf-thrust motor but is constructed with aluminum 6061-T6 material (designed to a minimum safety factor of 1.5) and has a total inert weight of 20 lbs. A diagram and an exploded drawing of the flight-weight motor are shown in Fig. 3.
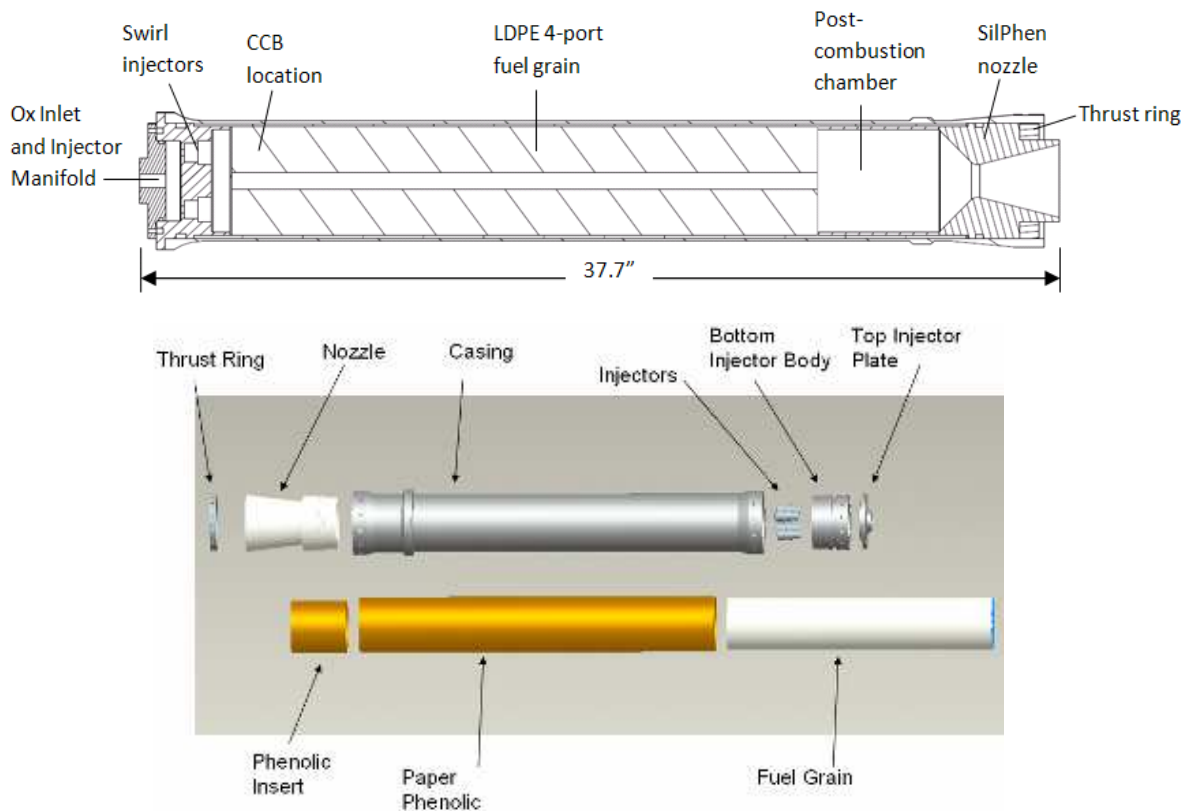

Figure 3. Diagram and exploded view of the 900 lbf-thrust flight-weight hybrid rocket motor.

Oxidizer enters the motor through the injector manifold assembly, which distributes the peroxide into four injectors. Each injector is sized to provide 0.9 lb/sec of oxidizer mass flow rate, with a 20% system pressure drop. The spray cone angle and nozzle orifice exit plane were designed such that the oxidizer impinges on the inside of the star shaped surface of the consumable catalyst bed (CCB) ignition system. The CCBs, previously invented at Purdue, cause hydrogen peroxide to decompose upon contact thus providing the necessary energy to initiate combustion of the H_2O_2/LDPE propellant combination. There are four CCBs located directly downstream of the injectors, mounted on the inner surface of the four LDPE fuel grain ports.

The conical nozzle is made from high-temperature composite silica-phenolic. This material allows for ablative cooling with an average regression rate of 0.005 inches per second at the throat. The chamber itself is lined with paper phenolic tubing, which provides both the primary seal and insulation for the motor. Sealing on the forward end is provided by a butt-seal between the phenolic liner and the injector manifold. A similar butt-seal is created with the nozzle at the aft end of the motor. Viton o-rings placed at either ends of the motor provide a secondary seal. The post combustion chamber and the injector face plate are thermally protected with carbon-filled EPDM

insulation and RTV sealant. High temperature RTV sealant is also applied to the butt-seal joints for additional insulation and sealing.

The injector manifold at the forward end of the motor is secured with machine screws, while the nozzle and thrust ring at the aft end are held in by shear pins. Along with the motor, a flight-weight oxidizer tank was also constructed from aluminum 6061-T6 and weighs in at 12 lbs. The tank uses double piston o-ring seals and both endcaps are secured with fasteners. It has a maximum expected operating pressure (MEOP) of 550 psia, a proof pressure of 850 psia and a burst pressure of 1050 psia. FEA was used for stress analysis, and the tank was subjected to hydro-testing at proof pressure levels (1.5 X MEOP). The forward end of the tank is fitted with a vent valve assembly, which contains a solenoid vent valve, a relief valve, and a pressure transducer. A photo of the flight-weight motor and tank assembly is shown in Fig. 4
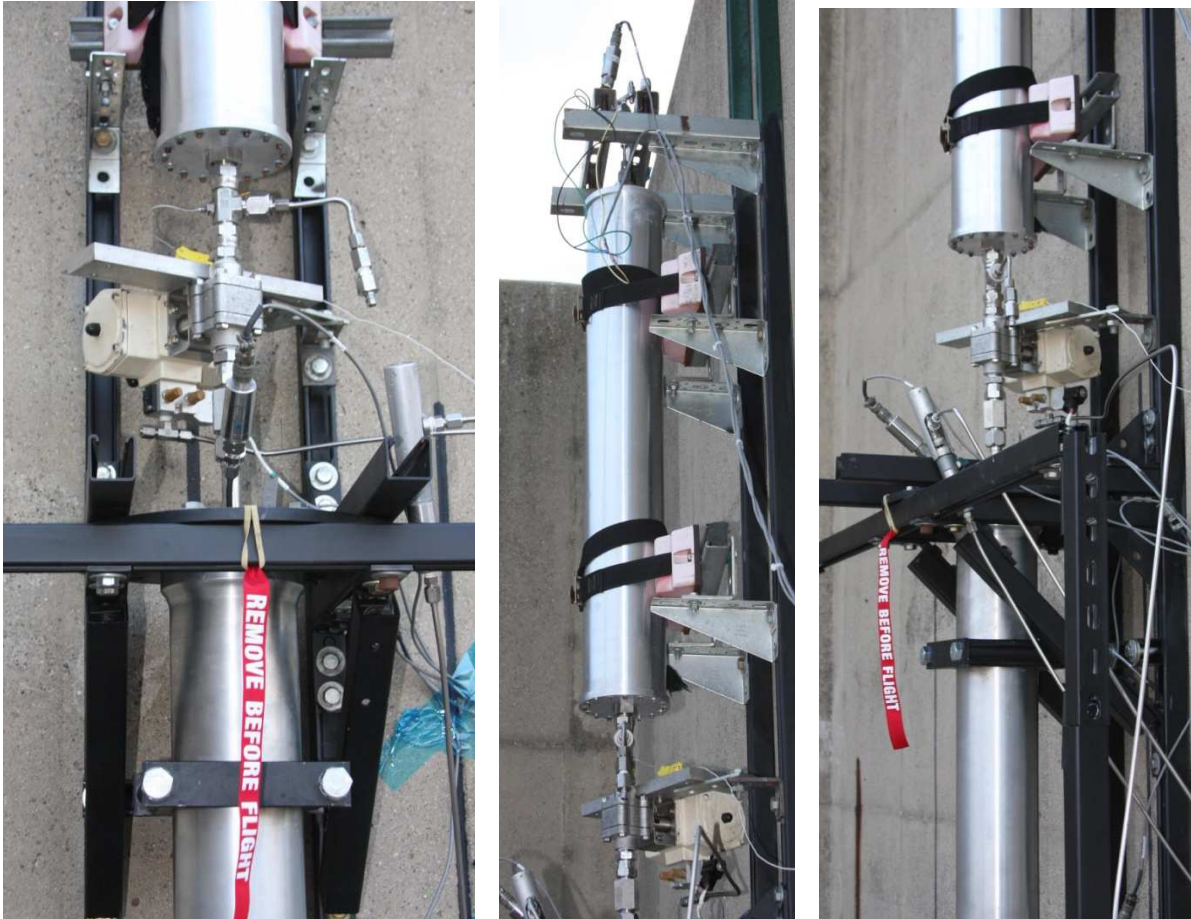

Figure 4. Flight-weight motor, valve and oxidizer tank assembly for hot-fire testing.

The hybrid motor, oxidizer tank, and all associated plumbing are housed inside the seven-foot carbon fiber booster section. Peroxide loads into the vehicle via a quick-disconnect (QD) valve which protrudes through the aerostructure below the tank. Just downstream of the QD valve is the main 3/4" ball valve. Its stem is fitted with an adapter lug which protrudes from the vehicle to allow for external actuation. Although all other pneumatics on the launch platform are charged with nitrogen, the main valve requires helium for faster actuation – this avoids the possible startup scenario where enough thrust is generated for the vehicle to lift off before the ball valve has completed its turning. A cavitating venturi located downstream of the main valve prevents a surge of hydrogen peroxide from injecting into the chamber during motor start-up. During ground testing, transducer readings are available for tank ullage pressure, injector inlet pressure, and chamber pressure. Thermocouples are also placed at critical locations to monitor the temperature of hydrogen peroxide. When the propulsion system is fully integrated into the carbon fiber aerostructure, only the tank ullage pressure measurement is taken. A plumbing and instrumentation diagram (P&ID) for the GSE and flight-vehicle is provided in the appendix.

American Institute of Aeronautics and Astronautics

B. Hot-Fire Testing

Prior to hot-fire testing of the motor, injector pressure drop and mass flow calculations were performed in order to determine the desired oxidizer tank ullage pressure, amount of oxidizer to be loaded, and run times. In order to fully characterize the injectors, a total of 13 cold flow tests were performed in June and July of 2008. Nine of these tests were performed on the battleship motor injector assembly, while the remaining 4 tests were performed on the flight-weight injector. A picture of the flight-weight injector assembly during cold flow testing is shown in Fig. 5.

Figure 5. Injector cold flow tests on the flight-weight injector manifold assembly. Notice the disengaged quick-disconnect assembly on the right-hand side of the picture.

In Fall 2008, a series of five hot-fire tests were performed on the vertical test stand at the Purdue High Pressure Lab. The goal of this test series was to check the performance of the new flight-weight motor, as well as to verify the operation of the new flight-weight tank, the Ground Support Equipment, the avionics hardware, and the LabView data system. A photo of the setup is shown in Fig. 6. The first two tests were run with the battleship motor (which had already been hot-fired over 15 times in a horizontal configuration), and the next three tests made use of the 900 lbf thrust flight-weight motor. The purpose of these tests was to ensure the structural and thermal integrity of the flight-weight motor under hot-fire test conditions, and to obtain critical performance data.
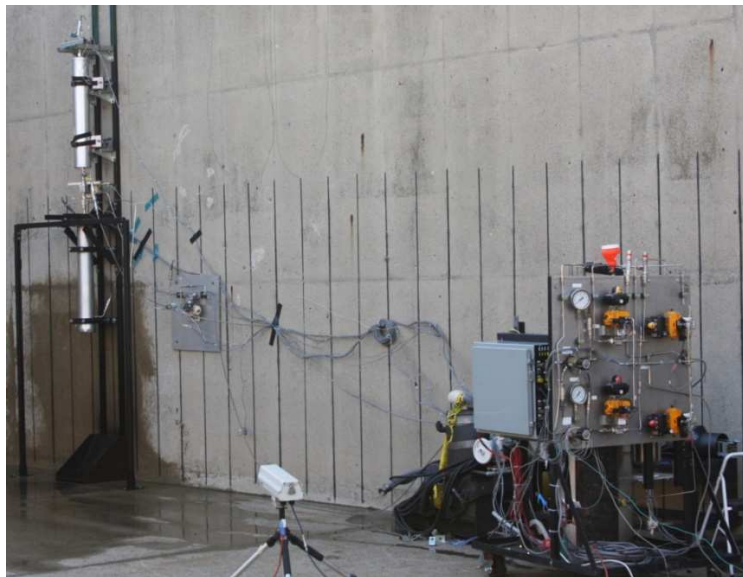

Figure 6. Vertical hot-fire test setup. The vertical test stand with the flight-weight motor and tank is shown on the left, while the GSE is shown on the right.

Results from the Fall 2008 test series are presented in Table 1. Flight-weight motor tests #4 and #5 were intended to simulate motor operating conditions to be used on the first launch. As expected, flight-weight motor performance was very similar to the battleship motor tests, with an oxidizer-rich O/F ratio ranging between 9 and 11 (optimum is 7.0), a c* efficiency of approximately 90%, and an average specific impulse of 188 seconds. Peak specific impulse of around 193 seconds is seen after start-up.

Table 1. Hot-Fire Test Series Summary using blow-down pressurization system. Performance numbers are time-averages.

Test	Motor	Burn Time	Throat Diameter	Chamber Pressure	O/F	c*	Isp	Thrust start - end
1	Battleship	3.9 s	1.62 in	236 psi	11.0	4384 ft/s	175 s	750 - 600 lbf
2	Battleship	6.5 s	1.38 in	224 psi	9.1	4573 ft/s	189 s	680 - 350 lbf
3	Flight	2.2 s	1.75 in	213 psi	11.1	4471 ft/s	174 s	900 - 600 lbf
4	Flight	5.4 s	1.42 in	236 psi	9.3	4514 ft/s	187 s	800 - 400 lbf
5	Flight	5.5 s	1.41 in	241 psi	9.2	4524 ft/s	189 s	800 - 400 lbf

Pressure histories from hot-fire test #4 are shown in Fig 7. There is an average pressure drop of 7% between the tank and the injectors (this includes the main valve and venturi), and 21% between the injector manifold and the chamber. Large transients in the first second are typical of the violent decomposition of the CCB ignition system. The pressure transducer located downstream of the cavitating venturi is picking up ignition spikes due to its close proximity to the CCBs.
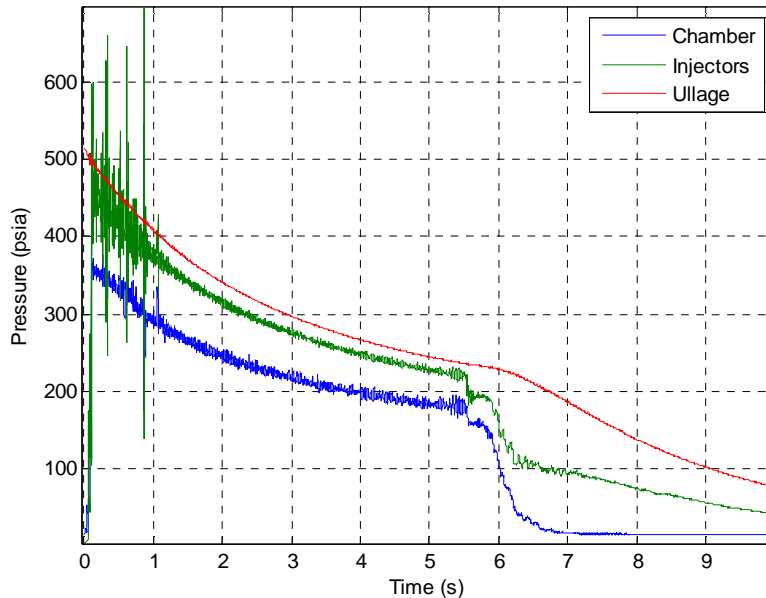

Figure 7. System pressure traces for flight-weight motor, hot-fire test #4.

Figure 8 shows the thrust curves for each of the five hot-fire tests. Thrust was not directly measured but was calculated using pressure and flow rate data. Fuel flow rates were calculated using the hybrid burning rate law ($\dot{r} = aG_o^n$),[1] in which the coefficient *a* was adjusted until the code predictions for final port diameter and fuel mass exactly matched post-test measurements. The characteristic velocity is determined as a function of O/F ratio based on NASA's 1-D thermochemistry code, CEA. As expected, the burn times increased and the "blow-down" was more extreme with reduced throat areas. Hot-fire tests #4 and #5 were prepared with identical throat areas and peroxide loads, which resulted in very consistent and repeatable thrust curves.
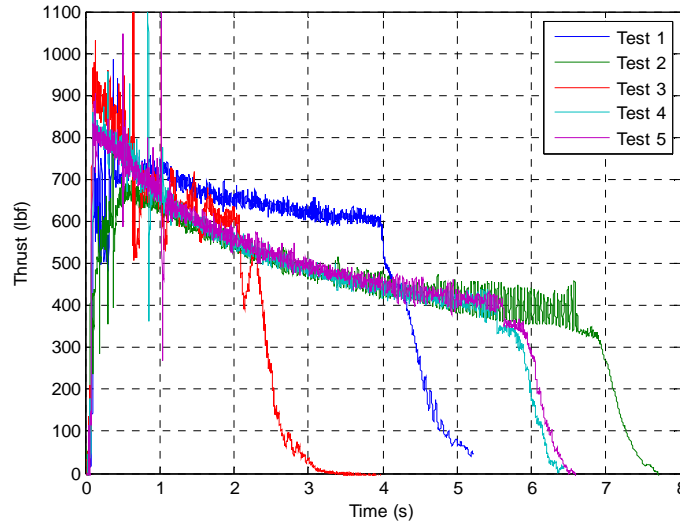
Figure 8. Calculated thrust from the Fall 2008 test series.

Hybrid rocket motors in general are prone to significant O/F shifts due to the inevitable change in fuel grain port geometry as the burn progresses. The H_2O_2/LDPE combination, however, has been shown to have a burning rate law exponent very close 0.5,[2] a case in which the decrease in oxidizer flux rate is offset by the increase in port surface area. Fig. 9 shows a plot of the O/F ratio from the Fall 2008 hot-fire tests. The decrease in O/F that is present in these tests may be attributed mostly to the decreasing oxidizer flow during blow-down conditions. This drop in O/F is actually favorable to the performance of the motor, since it operates ox-rich to begin with. As a result, c* increases by 6% across the burn (for hot-fire #4), which helps to offset the dramatic decrease in flow rate.
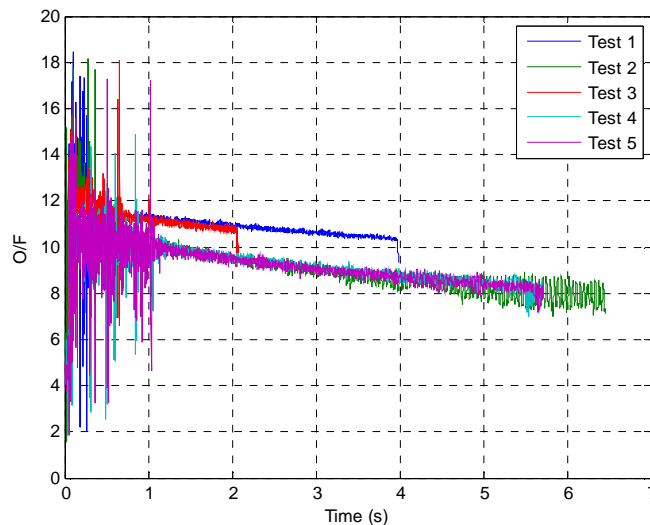
Figure 9. Calculated O/F shift from the Fall 2008 test series.

Table 2 presents the average regression and oxidizer flux rates, as well as the ratio of final to initial O/F and oxidizer flow rate. Fuel regression rates of approximately 0.020 inches per second are seen, which is consistent with other H_2O_2/LDPE tests in this regime.[2] There exists a clear relationship between the extent of the blow-down in

oxidizer flow rate and the severity of the O/F shift. Future versions of the hybrid motor will be operated in a pressure-fed configuration, thereby drastically reducing the change in O/F ratio during the burn. Upgrades will also be made to move the nominal O/F ratio closer to its optimum value.

Table 2. O/F ratio Shift and Regression rate data

Test	Average Regression Rate	Average Oxidizer Flux Rate	$(\dot{m}_{ox})_{final} / (\dot{m}_{ox})_{initial}$	$(O/F)_{final} / (O/F)_{initial}$
1	0.022 in/s	0.52 lb/in^{2}s	0.81	0.90
2	0.018 in/s	0.35 lb/in^{2}s	0.33	0.56
3	0.022 in/s	0.55 lb/in^{2}s	0.69	0.83
4	0.019 in/s	0.38 lb/in^{2}s	0.59	0.75
5	0.019 in/s	0.38 lb/in^{2}s	0.56	0.75

For these short-duration tests only about 15% of the fuel grain was actually used up. Fig. 10 shows the fuel grains from hot-fire tests #4, #5, and the integrated vehicle test along with a new grain. The ports take on an ovular shape after the burn, which is believed to be a result of a slight misalignment between the injector tips and each port. Measurements taken at the beginning, middle, and end of each port do not clearly point to a higher regression rate at any particular axial location. However, the first two inches of each port show very uneven burn patterns before transitioning to a smooth and uniform surface. This is likely due to the injector spray impinging slightly below the beginning of the port. Images of flight-weight motor hot-fire test #5 are shown in Fig. 11.

Figure 10: Fuel grains from Hot-fires #4, #5, and the integrated vehicle test along with a new grain. Top view of fuel ports (left image) and bottom view of fuel ports (right image).
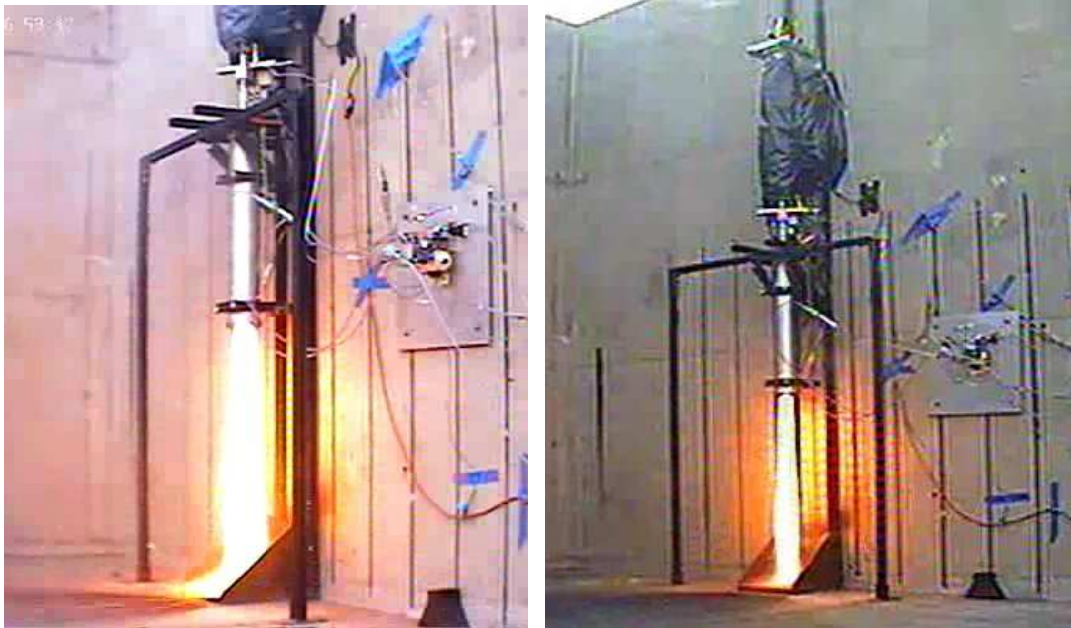
Figure 11. Hot-fire test #5 of flight-weight, 900 lbf thrust hybrid rocket motor, at Purdue High Pressure Lab.

III. Flight Vehicle Design

A. Vehicle Design and Structural Analysis

All vehicle subsystems such as propulsion, avionics and recovery are housed inside the vehicle aerostructure. The primary structural elements are designed to be re-usable and able to withstand multiple launch and recovery cycles, during which the vehicle is exposed to both external aerodynamic loads (drag, flutter, wind gusts, etc) as well as internal loads (thrust, acceleration, internal chamber pressure, motor vibration, and parachute ejection shock). At the same time, the structural elements have to be light-weight enough to enable the vehicle to achieve a sufficient thrust-to-weight ratio in order to obtain a safe rail exit velocity for fin guidance to become effective and for the vehicle to achieve its desired altitude and velocity requirements.

The aerostructure consists of four, 6" diameter sections of 0.08" thick carbon-fiber tubing and which are connected together with three, 1 ft sections of carbon-fiber couplers. The total length of the vehicle is 15.9 ft of which 8.25 ft consist of the nose cone, recovery, and avionics modules and of which 7.65 ft consist of the booster (pressurization and propulsion) section as shown in Fig. 12. A 2.5 ft length fiberglass conical nosecone is placed on the forward end of the vehicle and four carbon fiber fins are attached to the aft end of the vehicle to provide aerodynamic stability. The four fins are attached with carbon-fiber plain weave cloth. Wet hand layup technique was used to apply the cloth from the fin-tip to the fuselage and to the next fin-tip. After the layup process, vacuum bagging provides pressure on the composite layer assembly in order to improve bonding strength and remove excess resin as shown in Fig. 13.

The hybrid motor is secured to the vehicle via an aluminum thrust ring and rigid oxidizer feed lines. Upstream of the motor is the main and quick disconnect valves. Located further upstream is the 3.6 gallon hydrogen peroxide tank. The recovery/avionics modules are attached to the forward end of the oxidizer tank module through a 12" carbon-fiber coupler. The vehicle gross-lift-off-weight (GLOW) for the initial blow-down flight is 115 lb, consisting of 14.4 lb H_2O_2 propellant/pressurant, a 9 lb LDPE fuel grain and 91.6 lb of inert mass. Various structures for mounting and support are attached to the aerostructure. An aluminum ring is epoxied inside the carbon fiber tubing forward of the oxidizer tank to react axial forces as well as for attaching the Kevlar shock cords from the drogue parachute compartment. A stringer insert made of Aluminum provides additional stiffness to resist bending moments near the booster section coupler. An aerodynamics shroud built from fiberglass houses umbilical cords and the quick-disconnect (QD) device on the exterior of the carbon-fiber airframe.
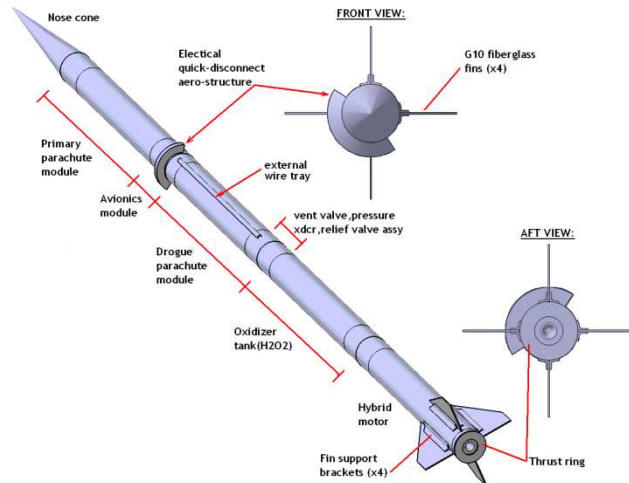
American Institute of Aeronautics and Astronautics

Figure 12. Schematic of the hybrid flight-vehicle.

Figure 13. Carbon-fiber wet hand layup (left) and vacuum bagging of fin assembly (right)

Recent work in vehicle modeling is focused on creating a system level finite element model (FEM) to be used in static and dynamic analyses. The intent is to predict propulsion system interface loads on and between the motor, feed line and oxidizer tank to ensure an adequate factor of safety is maintained at predicted worst-case scenarios. The propulsion system is modeled using NASTRAN CBEAM elements as shown in Fig. 14. The aerostructure, which includes the nosecone, body tubes, avionics collar, and fins, is modeled using NASTRAN CQUAD4 elements as shown in Fig. 14. Since only displacements and stresses of the propulsion system are of interest, the aerostructure FEM uses a courser mesh and estimates the carbon fiber lay-up using generic values. It is assumed here that a sufficiently stiff aerostructure model will transfer load in a similar fashion to the actual structure. The propulsion system and aerostructure are then connected using constraint elements and springs. Spring stiffnesses are selected based on engineering judgement. The top three connections use soft springs for vertical movement and rotation about the axis and stiff springs for transverse movement. This models the slip connection between the aluminum pressure vessels and the carbon fiber body tube. The aft motor restraint uses stiff springs in all DOF, representing a bolted connection. The vehicle system model uses 1855 elements and 1864 nodes.

Concurrently a CFD model is being created to determine the pressure distribution on the aerostructure. Using FEMAP or other commercially available software the pressure distribution from the CFD model can be interpolated onto the FEA model. The FEA model is then run in a dynamic load case with appropriate inertial loads. Loads recovered at points of interest will applied to the detailed FEM of the motor and oxidizer tank. In addition, flutter analysis is being performed on the vehicle fuselage and fins in order to assess whether the vehicle is operating in a regime where aero-elastic effects can be detrimental to vehicle structural integrity. This analysis allows a deeper

understanding of the flight-vehicle structure and also builds the foundation for creating similar analysis on future versions of the flight-vehicle.
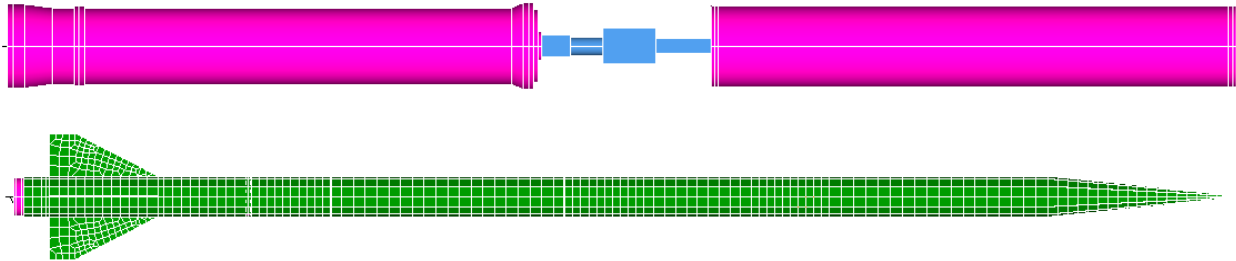

Figure 14. Propulsion system and flight-vehicle FEA models (upper and lower image).

Integrated vehicle, hold-down, hot-fire testing was performed at the High Pressure Lab by strapping down the entire flight-vehicle and performing launch operations with all avionics and GSE systems in flight configuration as shown in Fig. 15. This test served to load the vehicle aerostructure under full motor thrust and vibration, while also providing an opportunity to conduct a pre-flight rehearsal of all launch operations. Although no motor data was recorded, the hot-fire test ran smoothly and gave confidence in the integrated flight system.
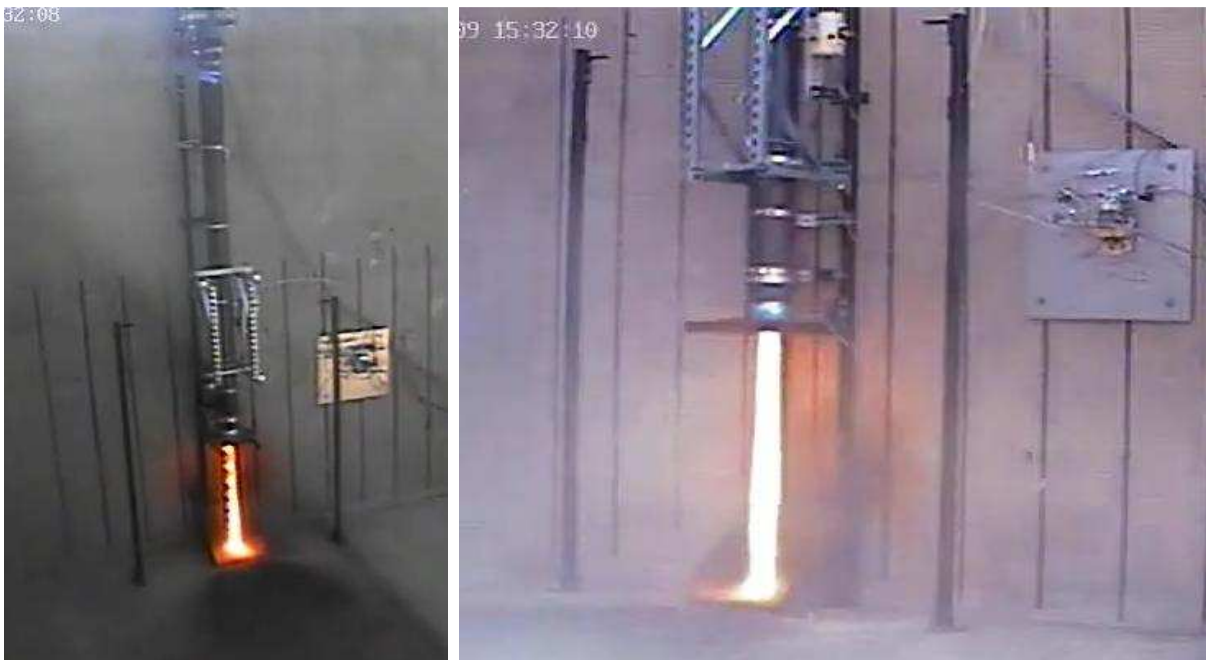
Figure 15. Full duration, integrated flight-vehicle, hold-down hot-fire test at Zucrow High Pressure Lab.

B. Aerodynamics

Both in-house developed codes and commercial off-the-shelf software are used to perform aerodynamics analysis on the vehicle. The Missile DATCOM code performs drag predictions at both subsonic and supersonic flight regimes. RockSim v.8 and Pro versions are also being used to perform basic drag simulations. The NASA vLoads code will be employed in order to obtain pressure distributions along the external surfaces of the vehicle which will in turn be passed on to the structures group for performing detailed FEA analysis on the primary aerostructure.

Static and dynamic stability analysis is mainly being performed by the use of RockSim v8 code. However, alternate codes are being sought to complement this analysis. The RockSim code requires the input of mass and geometry parameters for each component (propellant tank, motor, external carbon-fiber aerostructure, interstage couplers, etc). The motor thrust profile, tower launch angle, wind speeds, temperature and other launch factors are

inputted in the code as well. The code simulates the trajectory being followed by the flight vehicle in 2-D, and outputs position, velocity and acceleration vs. time for the entire flight. The code will output angle-of-attack, corrective moment coefficients, damping moment coefficients, static stability margins, normal force coefficients, and more versus time. Extensive simulations are being performed to ensure vehicle stability at all Mach numbers and at various atmospheric conditions (wind speeds, temperatures, thermal gradients, etc.)

In addition to software prediction of aerodynamic parameters, the flight vehicle aerostructure and its subscale models have been subjected to wind tunnel testing. Two models of lengths 1 ft and 1.5 ft were produced with a rapid prototyping machine. Each model was tested in a low-speed wind tunnel at different velocities and angles of attack in order to establish correlations for drag coefficient as a function of Reynolds number as shown in Fig. 15. A main observation was that as the Reynolds number increased, the C_D decreased following a 2nd order polynomial. As seen from Fig. 16, the test data from the small and large model fell beneath the predicted C_D based on other empirical data[3]. The vehicle aerostructure itself was tested in Purdue's Boeing wind tunnel which has a 4 x 6 ft test section and is capable of speeds up to 110 m/s (shown in Fig. 17).

Figure 15. Subsonic wind tunnel testing of sub-scale vehicle model.
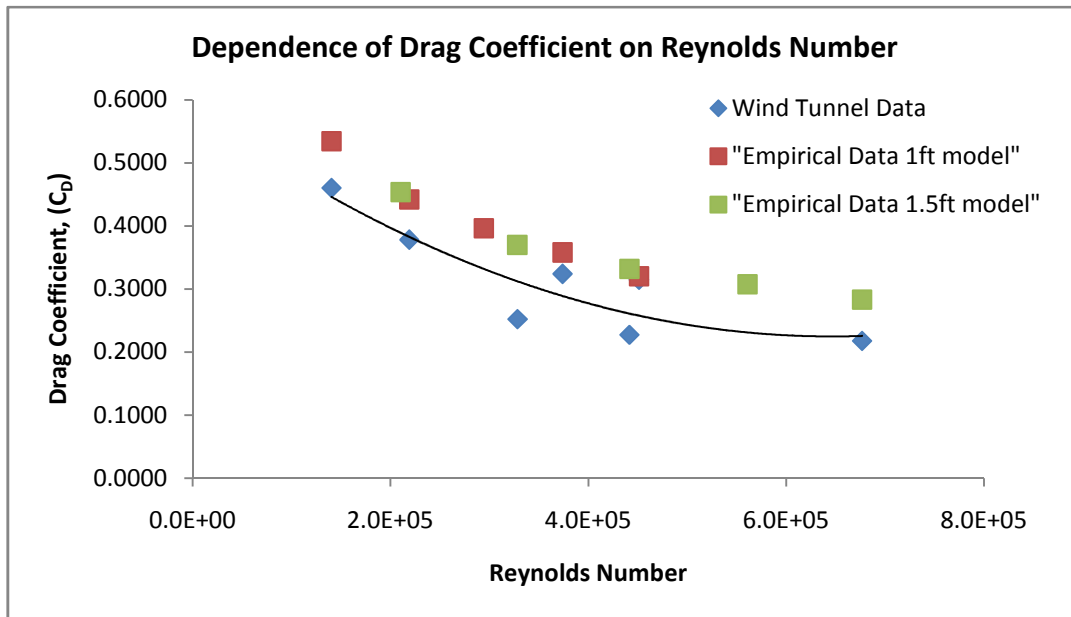

Figure 16. Wind tunnel data from both models matches empirical data to within approximately 14%

American Institute of Aeronautics and Astronautics

Figure 17. Subsonic wind tunnel testing of full scale flight-vehicle. The length of aerostructure was reduced to fit inside test section.

C. Trajectory Simulations

In addition to using Rocksim Pro as a analysis tool we decided to develop our own six degree of freedom trajectory simulation. The Sub-Orbital Rocket Dynamics Simulator (SORDS) is the final result of this endeavor. SORDS provides a platform where numerous rocket specifications including but not limited to thrust curves, inertia properties, mass history, and aerodynamic coefficients can be input and an accurate history of the rockets predicted translational and rotation will be output. SORDS was verified by ensuring that results were similar to that seen by Rocksim Pro. Further verification efforts are in progress. Currently SORDS features two different simulation modes. A single trajectory mode is available where a single flight simulation is run and can be extensively analyzed. Monte Carlo mode allows multiple trajectories to be run. Initial conditions for Monte Carlo mode are based on a random Gaussian distribution and output is in the form of a Google Earth Scatter of possible landing sites.

Single trajectory analysis for low wind speeds suggested that apogee would occur at approximately 6000 ft. A Monte Carlo analysis was carried out using ballistic trajectories in order to determine if the launch site was placed a safe distance away from nearby buildings. This analysis was setup with variance in wind speed and initial launch conditions. The results of our analysis suggested that for a constant speed, constant direction wind that the maximum safe launch wind speed would be 10 mph. This allowed a safety factor for measurement errors and slight change of wind between measurement and launch. An example of a Monte Carlo output from SORDS is shown in Fig. 18.
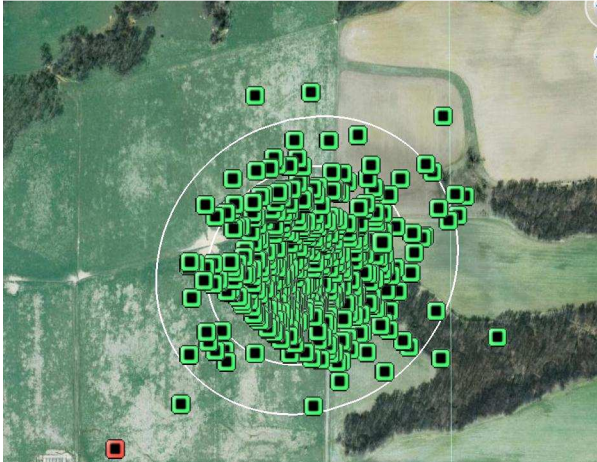

Figure 18. Monte Carlo simulation output from the SORDS code. The red marker is the launch site, and all green markers represent possible landing sites.

D. Avionics and Recovery System

The recovery system consists of dual parachute deployment, with drogue parachute ejection at apogee and primary parachute ejection at a predetermined altitude. System redundancy is achieved by use of two completely independent recovery modules for parachute ejection, with each module containing a lithium-ion battery, an R-DAS flight computer, and two redundant pyrotechnic ejection charges. The avionics module houses the on-board flight computers, altimeters, relays, batteries, and routers as shown in Fig. 19. The two redundant R-DAS flight computers

American Institute of Aeronautics and Astronautics

perform a number of functions including logging of altitude, velocity, and acceleration data in all three axes during flight. In addition they detect apogee and send a signal for drogue parachute deployment. At a predetermined altitude, they also command the ejection of the main parachute. Umbilical cords connect the GSE to the avionics (shown in left image of Fig. 19) which are then routed directly to control circuits for vent valve actuation, as well as relay of pressure transducer and temperature thermocouple data back to the GSE. One relay is used to control the opening and closing of the on-board oxidizer vent valve. The control circuits are powered by three 9V batteries. The GSE controls whether the vent valve is powered by external or internal power. Continuity circuits are built into the avionics in order to confirm that all electrical umbilical cords are connected properly to the flight-vehicle.

The drogue parachute module consists of a 6" diameter x 44.5" length carbon-fiber tube which contains the drogue parachute, 52 ft of nylon shock cord, 7 ft of kevlar shock cord, one piston assembly, one kevlar anti-zippering device, and associated stainless steel quicklink connectors. The drogue carbon-fiber tube is fastened to the avionics coupler via 4 expansion bolts. The drogue parachute has 6.3 ft^2 of surface area and a tested C_d value of 1.16. The primary parachute module consists of a 6" diameter x 47.9" length fiber-glass tube which contains the primary parachute, 76 ft of nylon shock cord, 7 ft of kevlar shock cord, one piston assembly, one kevlar anti-zippering device, and associated quicklink connectors. The primary parachute has 129 ft^2 of surface area, a tested Cd value of 2.92 and was sized to provide 15-25 ft/sec descent rates for the designed flight vehicle recovery mass. See Fig. 20 for layout of parts.
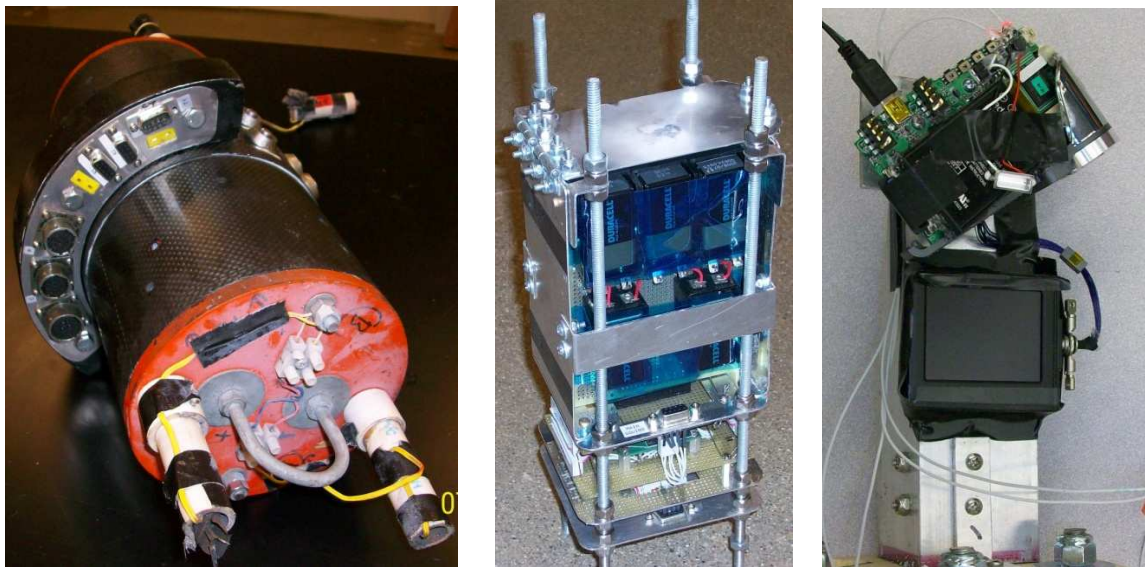

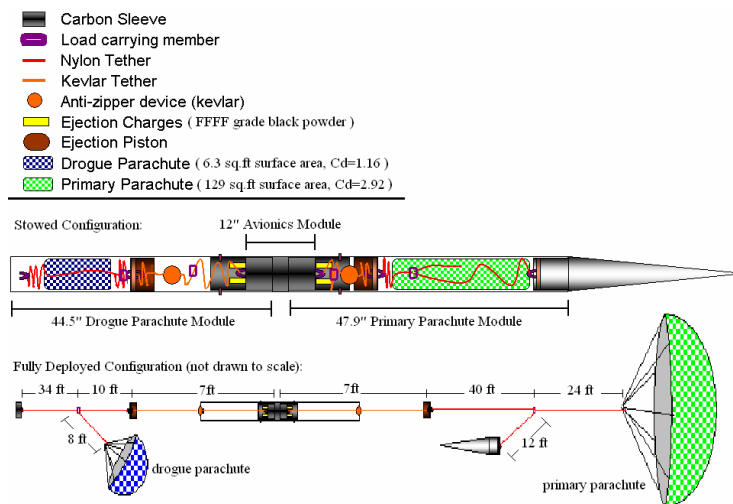**Figure 19. Avionics module (left), electronics chassis (center), and nose cone camera (right).**

Figure 20. Recovery system schematic.

American Institute of Aeronautics and Astronautics

The recovery sub-system was launched in October, 2006 powered by an AMW M-1900BB high-power solid rocket motor producing a maximum thrust of 520 lbf with a burn time of 3.23 seconds as shown in Fig. 7. The two onboard R-DAS flight computers recorded an apogee of 4700 ft, an average of 7.7 G's during the thrust phase, and a maximum velocity of 610 ft/sec (Mach 0.53). Successful deployment of the drogue parachute occurred at t+18 sec (apogee), providing an instantaneous deceleration of 12 G's. Both pyrotechnic charges fired. Successful deployment of the main parachute occurred as planned, at an altitude of 1300 ft (t+87 sec), providing instantaneous deceleration of 31 G's. Both pyrotechnic charges fired. Vehicle soft landing occurred perfectly at t+145 sec. The successful launch and deployment of the recovery sub-system concluded the recovery testing phase. Fig. 21 shows photos from the launch and recovery of this test flight.
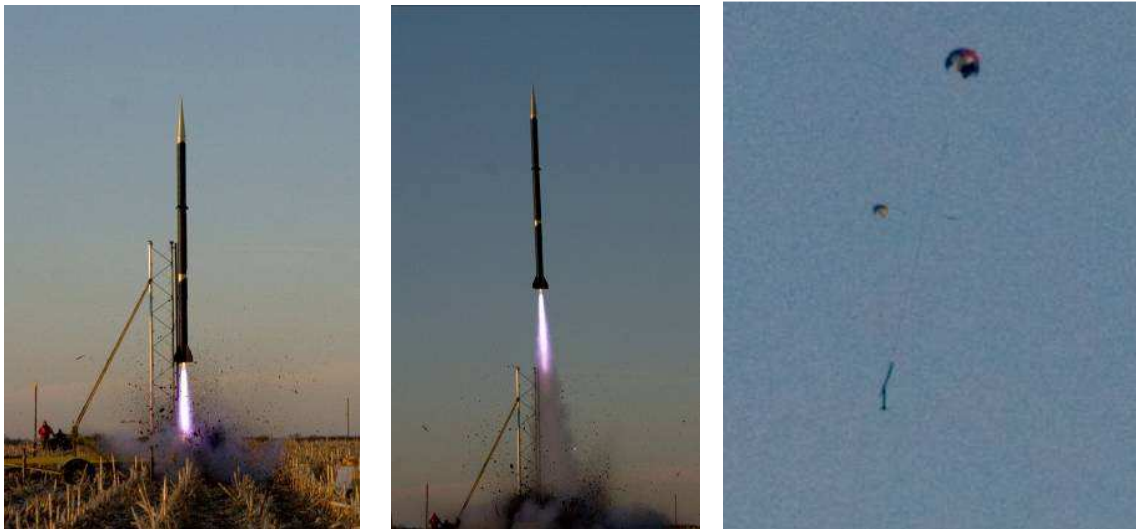

Figure 21. Successful launch and deployment of recovery system in October 2006.

E. Ground Support Equipment and Mobile Launch Platform

To allow the versatility of launching from multiple locations, the Ground Support Equipment (GSE) and launch rail are mounted on a utility trailer called the Mobile Launch Platform (MLP). The MLP is designed to transport the Ground Support Equipment to the launch area, interface with the flight-vehicle, and provide the initial guidance required for a stable flight. The deployable launch tower is made out of a 20-foot section of aluminum triangle truss with an attached unistrut rail. The tower houses the isolation panel and provides support for the flight-vehicle electrical umbilical cords and peroxide feed lines. Fig. 22 is a photo of the MLP with the launch tower deployed.

The ground support equipment (GSE) is used for controlling the remote loading and draining of hydrogen peroxide to and from the flight vehicle. Assembly and construction of the GSE was completed in 2006 and was subjected to water and hydrogen peroxide tests in 2007. Currently the system consists of five ½" H_2O_2 compatible pneumatically actuated ball valves, two dome loaded manual pressure regulators, two pressure relief valves, four pressure transducers, two thermocouples, four check valves and associated ¼" pneumatic and ½"oxidizer lines as shown in Fig. 22. Nitrogen is used to pressurize a hydrogen peroxide tank to the desired 600 psia ullage pressure in order to feed liquid oxidizer through a series of ball valves and into the flight vehicle propellant tank. Once propellant has been transferred into the vehicle, nitrogen is supplied for the blow-down pressurization through the same oxidizer fill line. The oxidizer fill line is disengaged from the vehicle by a remotely actuated quick-disconnect valve. To ensure safe launch operations, the oxidizer tank pressure and temperature are constantly monitored to verify that the hydrogen peroxide is not undergoing unexpected decomposition[4].

Launch is initiated by opening a normally closed, 3/4" ball valve which allows hydrogen peroxide to flow into the hybrid motor combustion chamber. In the event of an abort, the GSE has the capability of remotely draining the hydrogen peroxide into a dump tank located on the ground, by closing off the pressurization source, and opening the ½" dump valve. To ensure safety in launch operations, all circuits of the GSE and launch vehicle are designed to be fail-safe. In the event of an unexpected power outage, all solenoid valves return to their normal positions (normally open or closed) to allow venting of the tanks and automatic draining of the oxidizer from the launch vehicle directly into the dump tank. National Instruments Labview software is used for valve control and for monitoring system pressures and temperatures on the GSE/flight-vehicle systems. During ground testing, the Labview VI is operated

American Institute of Aeronautics and Astronautics

from the High Pressure Lab control room; during launch, a 1500-foot data cable and laptop are used. Fig. 23 shows the electronics module which contains the control and data acquisition systems for interfacing with valves, instrumentation and the laptop.
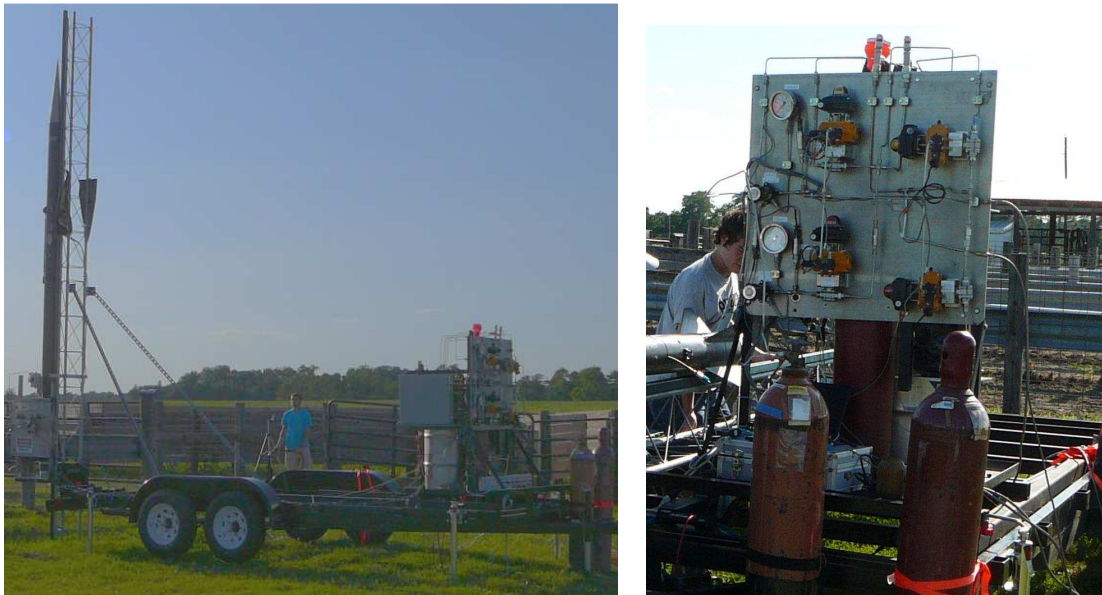

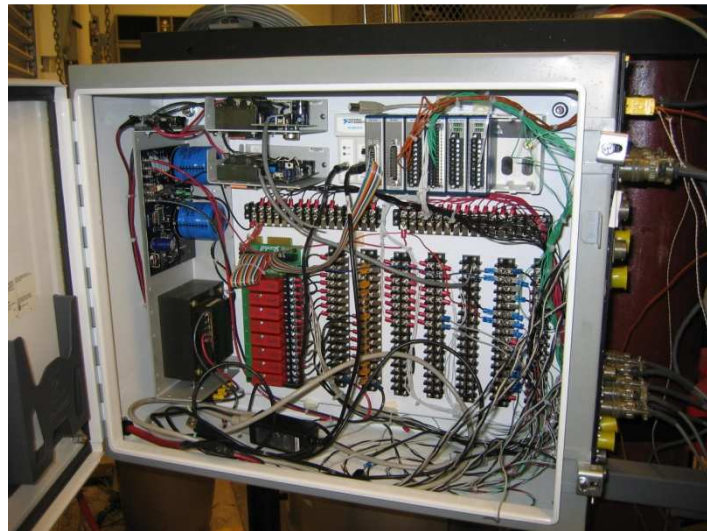**Figure 22. Mobile Launch Platform with deployable launch tower (left) and GSE equipment (right)**

Figure 23. GSE data acquisition and control electronics module

IV.   Launch of the Hybrid Flight-Vehicle

The inaugural launch of the Purdue Hybrid Rocket Technology Demonstrator took place in June 2009, from a remote site located approximately 12 miles west of West Lafayette, Indiana. The motor ignited as planned, produced approximately 800 lbf of initial thrust and lifted the 115 lb vehicle with an initial acceleration of 6Gs off the Mobile Launch Platform as shown in Fig. 24. The external valve actuator worked as planned, the avionics umbilical cords were retracted, and the fins cleared the MLP as designed. For the next 5.5 seconds the motor performed flawlessly as it consumed all of its 14.8 lbs of hydrogen peroxide while accelerating the vehicle to an altitude of approximately 6100 ft and producing a maximum velocity of Mach 0.6. Due to winds near 10 MPH, the flight-vehicle weathercocked into the wind, taking a trajectory which is normal at such wind conditions. Apogee

occurred at T+21 seconds, at which time the drogue apogee charges fired as planned. The shock from the apogee ejection charges caused the plastic shear pins of the nose cone to break and eject the nose cone prematurely. The main parachute which was tied to the nose cone therefore ejected at apogee and not at the pre-planned 700 ft altitude. The combination of drogue and main parachute deployment at apogee imposed larger-than-normal forces on the recovery harness. The recovery harnesses and quick-links, which are rated to over 1700 lbf, were able to withstand these loads.

At the instant that both parachutes deployed, the booster section was detached from the recovery harness and was not recovered successfully. This detachment was the result of the nylon tether severing on the forward bulkhead of the booster section. Nonetheless, the drogue, main, avionics and nose cone sections, which were still attached to both parachutes, slowly drifted away and were successfully recovered approximately 2 miles downrange (thanks to two on-board radio trackers they were easily found). The video camera successfully recorded high definition on-board video and the RDAS units recorded acceleration, velocity and altitude measurements taken throughout the entire flight. Data from the flight computer is plotted in Fig. 25.

Figure 24. Snapshots of hybrid flight-vehicle clearing launch tower under 6 Gs of acceleration, in ~0.4 sec.
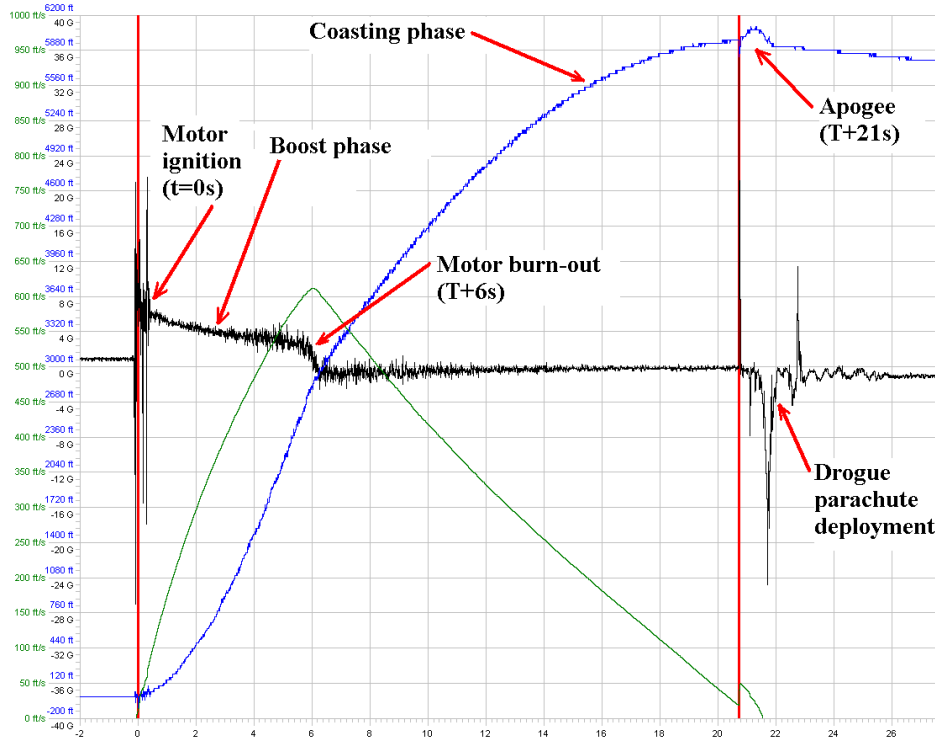
American Institute of Aeronautics and Astronautics

Figure 25. Plot of R-DAS flight data for acceleration (black), velocity (green) and altitude (blue).

Using the accelerometer data from the RDAS units and knowledge of the vehicle's mass, a thrust curve from the launch was computed. Fig. 26 shows this curve along with the calculated thrust from hot-fire tests #4 and #5, which were prepared with the same exact conditions as for the flight. The flight thrust curve lies closely to the hot-fire tests and confirms the expected performance of the motor. Overall, we are very pleased with the performance of the hybrid rocket motor, which delivered slightly more total impulse than was initially expected. The carbon-fiber aerostructures (fuselage and fins) were able to withstand the propulsive and aerodynamic forces as designed. In addition vehicle stability looked good throughout the boost and coasting phases of the flight. All avionics systems worked as planned, keeping the vehicle vent valve closed during motor operation, communicating with the GSE during launch operations, ejecting charges, logging data, and taking on-board video.
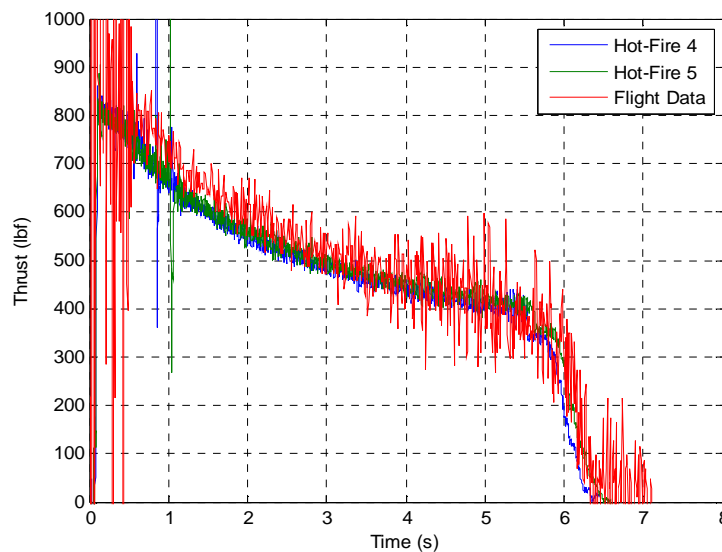

Figure 26. Flight-vehicle thrust profile plotted with thrust curves for hot-fire tests #4 and #5.

19
American Institute of Aeronautics and Astronautics

V. Conclusions

A 900 lbf-thrust H_2O_2/LDPE hybrid sounding rocket and all of its supporting systems have been designed, built, tested, and launched successfully to 6,100 ft. Recovery of the flight data revealed the vehicle performed close to predictions for its inaugural flight. Subsequent launches are planned for flying the vehicle in a pressure-fed configuration to altitudes exceeding 20,000 ft and reaching speeds in the supersonic regime. Construction of a Mobile Launch Platform and Ground Support Equipment provide the capability to launch safely from any desired remote location. Extensive simulation and testing of the different systems has also laid the groundwork for the future design of larger and more sophisticated hybrid flight-vehicles. To the authors' knowledge, the Purdue hybrid sounding rocket has been the largest hydrogen-peroxide hybrid rocket launched to date.
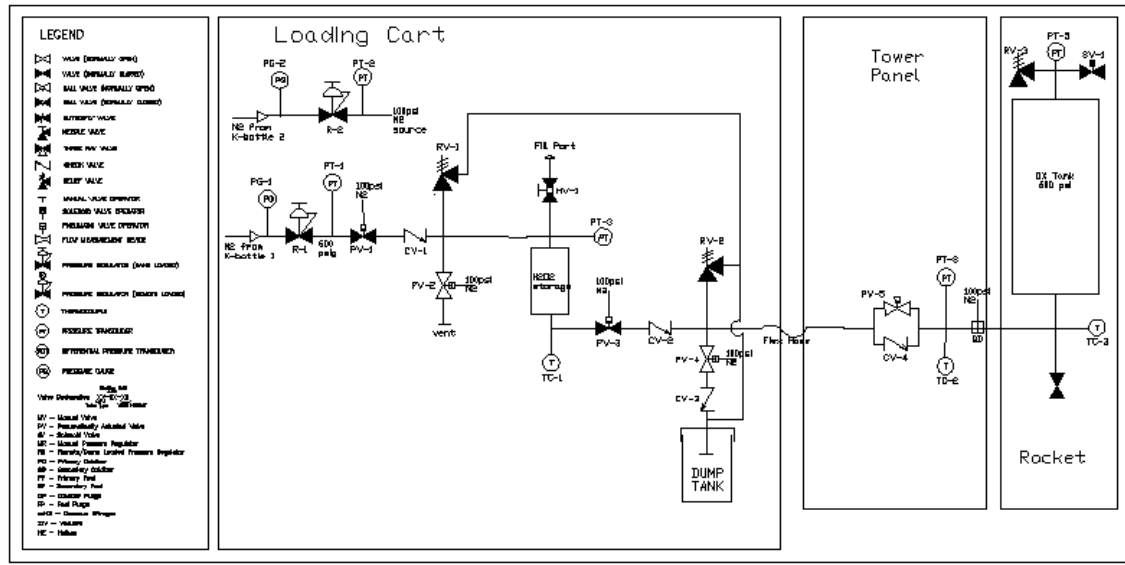
Appendix

Figure A1. Ground support equipment and flight-vehicle plumbing and instrumentation diagram.

Acknowledgments

References

[1]Humble, R. W., Henry, G.N., and Larson, W.J. (.ed), *Space Propulsion Analysis and Design*, Space Technology Series, McGraw-Hill, New York, 1995.

[2]Chiaverini, M. J., and Kuo, Kenneth K. (ed.), *Fundamentals of Hybrid Rocket Combustion and Propulsion*, Progress in Astronautics and Aeronautics Series, AIAA, Reston, VA, 2007, pp. 472.

[3]TR-11, Aerodynamic Drag of Model Rockets by Gerald M. Gregorek, published by Estes industries.

[4]Tsohas, J., Droppers, L., Case, E.G., Dambach, E., Heister, S. D., "Progress in Technology Demonstration for a Small Hybrid Launch Vehicle," AIAA RS5-2007-5004, 5th Responsive Space Conference, April 23-26, 2007, Los Angeles, CA.